

Study of the Long-Term X-Ray Variability of a Possible Quasar RX J0957.9+6903 with ASCA

Yu-ichiro EZOE¹, Naoko IYOMOTO², and Kazuo MAKISHIMA¹

¹*Department of Physics, University of Tokyo, 7-3-1 Hongo, Bunkyo-ku, Tokyo 113-0033*

E-mail(YE): ezoe@amalthea.phys.s.u-tokyo.ac.jp

²*The Institute of Space and Astronautical Science, 3-1-1 Yoshinodai, Sagamihara, Kanagawa 229-8510*

Abstract

Long-term variability and spectral properties of a possible quasar, RX J0957.9+6903, were studied, utilizing 16 ASCA observations spanning 5.5 years. The average 0.7–10 keV spectrum of RX J0957.9+6903 is well represented by a power-law continuum of photon index 1.58 ± 0.03 , and an absorption column of $\sim 1 \times 10^{21} \text{ cm}^{-2}$. The 2–10 keV flux of RX J0957.9+6903 varied by a factor of four over the period of six years, around a mean of $\sim 8.8 \times 10^{-12} \text{ erg s}^{-1} \text{ cm}^{-2}$. Peak to peak variability within each observation was less than 25% on ~ 1 day time scale. These properties support the classification of RX J0957.9+6903 as a quasar. The power spectrum density (PSD) was estimated in a "forward" manner, over a frequency range of $10^{-8.2}$ – $10^{-4.3}$ Hz, by utilizing the structure function method and Monte-Carlo simulation assuming a broken power-law type PSD. Then, the break frequency f_b of the PSD of RX J0957.9+6903 has been constrained as $1/f_b = 1600_{-1100}^{+\infty}$ days, and the logarithmic slope of the high-frequency region of the PSD as $\alpha = -1.55 \pm 0.2$. A comparison of the estimated PSDs is made between RX J0957.9+6903 and the M81 nucleus, observed in the same field of view.

Key words: Galaxies: active – Galaxies: individual (RX J0957.9+6903) – X-rays: galaxies – Methods: structure function

1. Introduction

Emission from an active galactic nucleus (AGN) is known to exhibit apparently random variability, over a wide wavelength range from radio to X-rays and γ -rays (e.g., Krolik et al. 1991; Edelson et al. 1996). Although the exact origin of such a variability is still unclear, it has been employed practically as a measure of the mass and size of the central black hole (BH) residing in the AGN. For example, Wandel & Mushotzky (1986) pointed out a strong correlation between the mass of the BHs in the AGNs estimated from optical emission lines, and the timescale of their X-ray variability in terms of the intensity doubling time. Hayashida et al. (1998) showed that the more luminous AGNs, which may have more massive central BHs, have longer timescale of variability; they utilized power spectrum density (PSD), which is mathematically more exact than the doubling time but suffers from the window function (the Fourier transform of the observational sampling) convolved with the true power spectrum of the source. These results indicate that the intrinsic X-ray variability timescale of AGN is an important parameter, which roughly represents the mass of the central BH.

Among AGNs, high-luminosity ones including quasars (QSOs) have such a long timescale of variability, e.g. a

few years, that the analysis of their variability timescale needs long observations. Such long observations in X-rays are generally limited to the all-sky monitoring of bright sources, including a limited number of QSOs (e.g., > 30 mCrab for RXTE, where "1 mCrab" flux is $\sim 3 \times 10^{-11} \text{ erg s}^{-1} \text{ cm}^{-2}$ in the 2–10 keV range).

RX J0957.9+6903, a possible QSO, has been observed as many as 16 times over six years from 1993 to 1999 with ASCA, in which the total exposure time reaches 620 ksec. This is because the object lies close to the spiral galaxy M81, and was always within the same field-of-view (FOV) in the repeated ASCA observations of SN1993J. This object was first detected in the Einstein observation of M81, and was designated M81 X-9 (Fabbiano 1988; Elvis et al. 1992), although it is not associated with M81. Subsequently it was observed with EXOSAT (Giommi et al. 1991) and ROSAT, and renamed RX J0957.9+6903 (Bade et al. 1998). It was identified optically with a faint point-like object having an extreme blue continuum (Bade et al. 1998) in the wavelength range between 3400 Å and 5400 Å. These optical properties suggest that RX J0957.9+6903 is a QSO, even though its cosmological redshift is still unknown. On the other hand, its association with a possible supernovae remnant (SNR), at a separation of $\sim 10''$, was proposed from an H_α observation (Miller et al. 1995).

In the present paper, we first study the 0.7–10 keV X-ray spectrum of RX J0957.9+6903 and variability in section 3, and show them to be consistent with those of a QSO. We then analyze the long-term light curve of RX J0957.9+6903 more quantitatively in section 4, and estimate its PSD utilizing the new method, developed by Iyomoto et al. (2000) and Iyomoto (1999) to study the long-term variation of the M81 nucleus. Because RX J0957.9+6903 and the M81 nucleus have always been in the same ASCA FOV and observed under the same sampling window, we can directly compare the estimated PSD of these two objects, one being a promising QSO candidate while the other a typical low-luminosity AGN (LLAGN).

2. Observation

We observed the M81 region 16 times with ASCA as summarized in table 1. It is among the objects most frequently observed with ASCA. We analyze only data from the GIS (Gas Imaging Spectrometer; Ohashi et al. 1996; Makishima et al. 1996) with FOV of 50' diameter, because our target, RX J0957.9+6903, was always outside the SIS (Solid-State Imaging Spectrometer) FOV in even the 4-CCD mode (22' \times 22' FOV). The GIS data were acquired in PH normal mode throughout.

For the GIS event selection, we required the geomagnetic cut-off rigidity to be $> 8 \text{ GeV c}^{-1}$ and the target elevation angle to be $> 5^\circ$ above the horizon. These criteria left us with 620 ksec of good GIS data. RX J0957.9+6903 was always detected, at a mean 0.7–10 keV counting rate of $6 \times 10^{-2} \text{ c s}^{-1}$ for each GIS detector (GIS2 or GIS3).

In figure 1 we show an example of the GIS images of the M81 region, after subtracting the non X-ray background. There were always two discrete X-ray sources in the GIS FOV; the brighter one (to the right in figure 1) is the emission complex from M81, while the fainter one (to the left in figure 1) is RX J0957.9+6903. The latter was detected at a J2000 position ($9^{\text{h}}57^{\text{m}}43^{\text{s}}, +69^\circ04'03''$), which is consistent with the J2000 optical position ($9^{\text{h}}57^{\text{m}}51^{\text{s}}.0, +69^\circ03'30''$; Bade et al. 1998) within the position accuracy of ASCA ($\sim 1'$; Tanaka et al. 1994). The M81 complex is elongated downward and upward because it consists of the nucleus (X-5) and three additional sources, SN 1993J, X-6, and X-4; these four sources are not resolved clearly from one another in the GIS image of figure 1. The results on SN 1993J have been reported by Kohmura (1994) and Kohmura et al. (1994). The results on the M81 nucleus of the 1st to 10th observations have been published as Ishisaki et al. (1996). The details of timing analysis of the M81 nucleus of all the 16 observations are published as Iyomoto et al. (2000).

3. X-Ray Properties of RX J0957.9+6903

3.1. Spectrum

For each observation, we accumulated photons within 3' of the X-ray centroid of RX J0957.9+6903 in the image and made spectra. The contamination from the M81 complex, estimated with the point spread function of the XRT (X-ray telescope), is less than $\sim 1\%$ of the total counts of RX J0957.9+6903 in this region, and can be negligible. Therefore, the background was taken from the same detector region in blank skies and subtracted, the count rate of which was an order of magnitude less than that of RX J0957.9+6903. The XRT+GIS response files were calculated separately for the two instruments (GIS2,3). We then added the GIS2 and GIS3 spectra into a single spectrum for each observation.

The obtained X-ray spectra of RX J0957.9+6903 are relatively featureless and all alike. In order to obtain a rough idea of the spectral variation, we fitted the 0.7–10 keV GIS (GIS2+GIS3) spectrum of individual observations with an absorbed power-law model. The absorption column density and photon index were taken as free parameters except the 16th observation. These 15 fittings were acceptable with the reduced $\chi^2 \sim 0.7$. The average absorption column density of these 15 spectral fittings was obtained as $\sim 9.5 \times 10^{20} \text{ cm}^{-2}$, which is higher than the Galactic line-of-sight column density of $4.06 \times 10^{20} \text{ cm}^{-2}$. The average photon index turned out to be ~ 1.6 except the 13th observation, when the photon index was 2.2. For the spectrum of the 16th observation, the column density became lower than the Galactic value and therefore was fixed at that Galactic value, which yielded an acceptable fit. The 2–10 keV fluxes and photon indices derived in this way from individual observations are shown in figure 2a and figure 3, respectively, as a function of time.

Because the spectral variation is thus negligible except the 13th and 16th observations, we summed up all the GIS (GIS2+GIS3) data except the 13th and 16th into a single spectrum. We calculated the average XRT+GIS responses as averages of those for individual observations weighted by respective exposure times. We also calculated the average background. Using these response and background, we fitted the summed GIS spectrum in the 0.7–10 keV range with an absorbed power-law model. This model was acceptable with the reduced χ^2 of 0.92. The obtained best-fit model is shown in figure 4 and the best-fit parameters are given in table 2.

As shown in figure 4b, a similarly good fit (reduced χ^2 of 0.75) to the average spectrum has been obtained by replacing the power-law model with a bremsstrahlung model of temperature $kT = 12.0 \pm 0.8 \text{ keV}$, with the absorbing column density fixed at the Galactic line-of-sight value. In table 2, we list these fit parameters as well.

3.2. Light curves

In figure 2a we present the background-subtracted long-term light curve of RX J0957.9+6903, in terms of the 2–10 keV flux as derived in section 3.1. Each data point corresponds to each of the 16 observations. Thus, the long-term variation amounts to a factor of ~ 4 (peak-to-peak), around an average flux of 8.8×10^{-12} erg cm $^{-2}$ s $^{-1}$.

To investigate the short-term variability, we subdivide each data point in the light curve into finer bins of 1/4 day width. Then, the peak-to-peak variation in each observation was found to be less than $\sim 15\%$ except the 13th observation, when it was 25%. Figure 2b shows the short-term light curve of the 13th and 3rd observations, the latter being the longest one. With this bin size, all the 16 observations constitute a 51-bin light curve. Typical 1σ error due to photon counting statistics is $\sim 4\%$ of the average flux, whereas root-mean-square (RMS) of overall variation through the entire light curve is much larger, 30% of the mean. This is important for our structure function analysis as described in section 4.1.

3.3. Comparison with the past observations

The flux of RX J0957.9+6903 measured in past observations is summarized in table 3. The results of the Einstein and EXOSAT data is quoted from Fabbiano (1988) and Giommi et al. 1991, respectively. The EXOSAT flux is converted from the countrate by utilizing the conversion factor in Fig 2 of Giommi et al. 1991. We extended the best fit power-law model of ASCA shown in table 2, to estimate the 0.2–4.0, 0.05–2.0 and 0.5–2.0 keV fluxes. Below we explain the ROSAT data.

We newly analyzed the three ROSAT PSPC archive data in table 3, which cover epochs between the Einstein and ASCA observations. The background-subtracted PSPC spectra of RX J0957.9+6903 are show in figure 5. The background spectra were taken from the blank field in the same FOV of each observation. These spectra were represented by an absorbed power-law model with the photon index ~ 2 and the absorption $\sim 2 \times 10^{21}$ cm $^{-2}$. The reduced χ^2 were 9/13, 5/10, and 21/16 for the 1991 May, October, and 1992 September observations, respectively.

Compared with the estimated ASCA fluxes, the Einstein, EXOSAT and ROSAT values are lower by a factor of ~ 1.5 . Considering, however, uncertainties of the cross-calibration between different instruments operating in different bands, and the RMS = 30% of the ASCA light curve, these fluxes measured previously can be thought to be within the variation range of RX J0957.9+6903.

3.4. The nature of RX J0957.9+6903

We have for the first time measured an accurate 0.7–10 keV spectrum of RX J0957.9+6903, and derived

short/long-term light curves. The obtained results, i.e., a power-law type spectrum with $\Gamma \sim 1.6$, small short-term variability and a significant long-term variability, are consistent with the past suggestion of RX J0957.9+6903 being a QSO (Fabbiano 1988; Ishisaki et al. 1996; Bade et al. 1998). These hard spectra and the random variability over ~ 6 years rule out the association of this object with an SNR (Miller et al. 1995). The object can not be a Seyfert galaxy since the optical counterpart is point-like (Bade et al. 1998). Although the featureless blue optical continuum is consistent with those of Blazars, the lack of a radio source within $\sim 1'$ of RX J0957.9+6903 (from NED) rules out its Blazer interpretation.

Although RX J0957.9+6903 has a high Galactic latitude ($\sim 40^\circ$), there still remains a small possibility that it is a Galactic object. The successful fit to the X-ray spectrum with a high-temperature Bremsstrahlung (figure 4b) leaves room for either a cataclysmic variable (CV) or a low-mass X-ray binary (LMXB); the former exhibits a genuine high-temperature thermal X-ray spectrum (e.g., Ishida 1991), while the latter an optically-thick spectrum which can be approximated by a mildly absorbed ($N_{\text{H}} \sim 1 \times 10^{21}$ cm $^{-2}$) high-temperature Bremsstrahlung (Makishima et al. 1989). The featureless blue optical continuum of RX J0957.9+6903 (Bade et al. 1998) is inconsistent with the CV interpretation, while consistent with the LMXB scenario where the optical emission mainly arises from reprocessed X-rays. However, in addition to the small number of high-latitude Galactic X-ray sources, its X-ray to optical flux ratio becomes $\log [f_{\text{X}}/f_{\text{B}}] \sim 0.9$ where f_{B} is the optical blue flux obtained from $m_{\text{B}}=18.6$ (Bade et al. 1998). This is low for an LMXB which would show $\log [f_{\text{X}}/f_{\text{B}}] \sim 2 - 3$; e.g., Ritter 1990, while consistent with that of QSO ($\log [f_{\text{X}}/f_{\text{B}}] \sim -1 - +1$; e.g., Tananbaum et al. 1979).

From these considerations, we conclude that RX J0957.9+6903 is a radio-quiet QSO. If, for example, the object lies at a redshift of 1.0, the 2–10 keV luminosity becomes 3×10^{46} erg s $^{-1}$, assuming the Hubble constant to be 70 km s $^{-1}$ Mpc $^{-1}$ and a flat universe without cosmological constant. This is reasonable as a QSO luminosity.

4. Structure Function Analysis

We obtained a 51-bin light curve with the 1/4-day bin width. Because of the sparseness of this light curve, it is difficult to determine the PSD of RX J0957.9+6903 directly by Fourier transformation. Therefore we utilized the "forward method" analysis incorporating structure function as developed by Iyomoto (1999) and Iyomoto et al. (2000). Below we briefly explain this method. Further details of this method are given by Iyomoto et al. (2000).

4.1. Structure function

For a time series of luminosity l_m , the first-order structure function (SF), $S(\tau_k)$, is given as

$$S(\tau_k) = \frac{1}{N(\tau_k)} \sum_{m=0}^{N-1-\tau_k} (l_m - l_{m+\tau_k})^2 \quad (1)$$

where l_n is the luminosity at time t_n and τ_k is the time lag between t_m and $t_{m+\tau_k}$. The sum is taken over those pairs which have the same time lag τ_k , and $N(\tau_k)$ is the number of such pairs. The general definition of SF is given by Simonetti et al. (1985). In the case of equally sampled data, SF and PSD are mathematically equivalent.

Figure 6a shows the SF of RX J0957.9+6903 calculated from the 51-bin light curve using equation (1). The statistical error of the light curve contributes little, because the RMS variation of the light curve is larger by an order of magnitude as described in section 3.2; the contribution of the Poisson noise to the SF is calculated to be $[(\text{Poisson error})/(\text{RMS})]^2 = (4/30)^2 \sim 2\%$. In figure 6a we can see that the various sampling intervals give the wide-band SF. The SF is smooth at short time lags because there are many pairs with such small time lags, or $N(\tau_k)$ is large. The SFs at large time lags scatter very much because of small values of $N(\tau_k)$. To suppress the scatter of SFs at large time lags, we have binned the SFs into 22 appropriate intervals as shown in figure 6b. Thus, the SF keeps increasing rather monotonically to longer time lags, indicating that the typical time scale of variation is long. Even using the binned SF, however, it is difficult to convert the SF into PSD because of the sampling window effect of the 16 observations. Therefore we utilize the forward method analysis.

4.2. Forward method simulation

As the forward method analysis, we begin with producing many Monte-Carlo light curves assuming a model PSD and the actual observation sampling window. We next convert each simulated light curve into a fake SF and then compare the ensemble average of those fake SFs with the SF derived from the actual data.

As the PSD model of RX J0957.9+6903, we assume a broken-power-law shape as

$$P(f) = \begin{cases} P_0 & (f < f_b) \\ P_0(f/f_b)^\alpha & (f > f_b) \end{cases} \quad (2)$$

where f denotes frequency, P_0 is a constant, f_b is a characteristic frequency called "break frequency", and α is a slope index. It is an empirical PSD of AGNs (e.g., Pounds & McHardy 1988; Edelson & Nandra 1999). We regard f_b and α as free parameters. The trial values of $1/f_b$ are $10^{1.0}, 10^{1.2}, 10^{1.4} \dots$ and $10^{3.4}$ days, and those of α are $-1.20, -1.25, -1.30 \dots$ and -2.40 . For each pair of

f_b and α , we generated 1000 fake light curves via Monte-Carlo method, by giving random phases to the Fourier components. Each fake light curve was subjected to the sampling window for RX J0957.9+6903, to make a simulated 51-point sparse light curve. Then we calculated an SF from each fake 51-point light curve.

Figure 6c shows the ensemble average of the 1000 simulated SFs, for $\alpha = -1.55$ and $f_b = 10, 100$, and 1000 days, without applying the sampling window. Comparing figure 6b with figure 6c, we can again estimate that the variation timescale of RX J0957.9+6903 is relatively long. Figure 6d shows the ensemble average of the 1000 fake SFs which were calculated after each simulated light curves was multiplied with the actual sampling window; it was subjected to the same binning as figure 6b, so that the simulation can be directly compared to the actual SF.

We compared the observed and simulated SFs by utilizing the χ^2 technique. The χ^2 is defined as

$$\chi^2 = \sum_{\tau_k} \frac{(S_{\tau_k}^{\text{Obs}} - \overline{S_{\tau_k}^{\text{Fake}}})^2}{\sigma_{\tau_k}^{\text{Fake}}} \quad (3)$$

where $S_{\tau_k}^{\text{Obs}}$ and $\overline{S_{\tau_k}^{\text{Fake}}}$ are the observed and the average fake SFs, while $\sigma_{\tau_k}^{\text{Fake}}$ denotes RMS of the 1000 fake SFs at time lag τ_k . We regard this χ^2 as a measure of goodness of the employed PSD model. Among various PSDs which have different values of f_b and α , we have obtained the best PSD for $1/f_b = 10^{3.2}$ days and $\alpha = -1.55$ with $\chi^2/\nu = 0.84$. We can regard the PSD with these parameters to be the best as long as assuming the model PSD of equation (2).

4.3. Uncertainties in the power spectrum density

We again utilized Monte-Carlo simulation to evaluate uncertainties in the PSD estimation. We generated another 1000 fake light curves using the best parameters, f_b and α , obtained in section 4.2. The random numbers of these simulated light curves are different from each other, and from those used in section 4.2. For each of the newly generated fake SFs, we determine the optimum f_b and α in the same way as for the RX J0957.9+6903 data, and derive the χ^2 value, χ_{min}^2 . We derived also χ^2 , χ_{true}^2 , on each simulation at the best-fit parameters of $1/f_b = 10^{3.2}$ days and $\alpha = -1.55$, obtained in section 4.2. We then calculate

$$\Delta\chi^2 \equiv \chi_{\text{true}}^2 - \chi_{\text{min}}^2 \quad (4)$$

for each light curve. Figure 7a shows the integrated distribution of $\Delta\chi^2$ from the latter set of 1000 simulations. We determine the 90% and 99% confidence regions from this distribution. In figure 8a, we show the obtained confidence regions on the 2-dimension plane of f_b and α . The best parameters with 90% confidence errors thus become

$1/f_b = 1600_{-1100}^{+\infty}$ days and $\alpha = -1.55 \pm 0.2$. Similarly in figure 8b, we present an overlay of various PSDs corresponding to the 90% confidence region of figure 8a. We can see a possible break in the PSD.

Utilizing the χ_{true}^2 distribution of the 1000 simulations, we can also estimate how well the assumed PSD expresses the RX J0957.9+6903 PSD. Figure 7b shows the distribution of χ_{true}^2 , where an arrow indicates the χ^2 value we have obtained from the SF of RX J0957.9+6903 in section 4.2. The χ^2 value of RX J0957.9+6903 is almost at the peak of this distribution, which justifies our assumption of equation (2).

4.4. Time scale of variation of RX J0957.9+6903

We have estimated the break frequency and slope index of RX J0957.9+6903 on the assumption of equation (2) which describes typical intensity variations in AGNs. Seyfert galaxies exhibit $f_b = 10^{-4} \sim 10^{-6}$ Hz and $\alpha = -1 \sim -2$ (e.g., Lawrence et al. 1987 for NGC 4051; McHardy, Czerny 1987 for NGC 5506; Hayashida et al. 1998 for NGC 4051 and MCG 6–30–15). From Galactic black hole candidates, we typically observe $f_b \sim 0.1$ Hz and $\alpha = -1 \sim -2$ (e.g., Makishima 1988). Our results for RX J0957.9+6903 are $f_b \sim 7.3 \times 10^{-9}$ Hz and $\alpha \sim -1.55$. This α value is consistent with those of typical AGNs. Furthermore, the variation time scale ($1/f_b$) of RX J0957.9+6903 is about 3 orders of magnitude longer than those of rapidly varying Seyferts. This long term variation resembles those of 3C273, a representative QSO (Hayashida et al. 1998).

Although the physical mechanism accounting for equation (2) is not yet understood, lower values of f_b are generally thought to imply higher central BH masses (e.g., Hayashida et al. 1998). If we further assume that the BH mass M_B is inversely proportional to f_b , it may be written as

$$M_{\text{BH}} = 10 \times 0.1[\text{Hz}]/f_b M_{\odot} \quad (5)$$

where 0.1 Hz and $10 M_{\odot}$ are the parameters of Cyg X-1 as a standard. Then our results on RX J0957.9+6903 imply $M_B > 10^8 M_{\odot}$. This value is in a typical range of mass of QSOs estimated from their luminosities, which are assumed to be close to the Eddington limit (e.g., Lawson & Turner 1997, Reeves et al. 1997).

4.5. Comparison with the M81 nucleus

Utilizing the same structure function method, Iyomoto et al. (2000) have analyzed the time variability of the M81 nucleus, an LLAGN, detected in the same FOV as RX J0957.9+6903 over these 6 years. Because the window function for RX J0957.9+6903 is the same as that for the M81 nucleus, we may directly compare the time scales of their variations. Iyomoto et al. (2000) have

found the inverse of the break frequency of the M81 nucleus to be larger than 800 days (90% lower limit), which is close to that of RX J0957.9+6903, $1600_{-1100}^{+\infty}$ days. Therefore the M81 nucleus (LLAGN) may have a central BH as heavy as that of RX J0957.9+6903 (QSO). This in turn suggests that the central BH mass of the M81 nucleus, and generally of other LLAGNs, is higher than those of the fast-varying Seyfert nuclei, and their very low luminosities are a result of extremely small accretion rates as argued, e.g., by Iyomoto et al. (1996), Ishisaki et al (1996), and Iyomoto et al. (1998).

5. Summary

RX J0957.9+6903 has been observed 16 times with ASCA over 5.5 years. The average 0.7–10 keV GIS spectrum is represented by a power-law continuum of photon index 1.58 ± 0.03 , and an absorption column of $\sim 1 \times 10^{21} \text{ cm}^{-2}$. Spectral variation was insignificant except the 13th and 16th observation. The 2–10 keV flux varied by a factor of four through 6 years, and the short-term variation was 25 % or less on a time scale of about one day. These results, together with the optical observation, support the interpretation of RX J0957.9+6903 as a QSO (Fabbiano 1988; Bade et al. 1998).

Through a forward-method analysis utilizing structure function, the PSD of RX J0957.9+6903 has been estimated to have a very low break frequency f_b , $1/f_b = 1600_{-1100}^{+\infty}$ days, and the slope index $\alpha = -1.55 \pm 0.2$. From the mass-timescale relation for various BHs, the central BH mass of RX J0957.9+6903 is estimated to be $> 10^8 M_{\odot}$. The comparison of the PSDs between RX J0957.9+6903 (QSO) and the M81 nucleus (LLAGN), estimated in the same way under the identical sampling window, indicates that the two objects have similar time scales of variation. This further supports that the central BH mass is not much different between QSOs and LLAGNs.

Reference

- Bade N., Engels D., Voges W., Beckmann V., Boller Th., Cordis L., Dahlem M., Englhauser J., Molthagen K., Nass P., Studdt J., Reimers D. 1998, A&A 127, 145
- Edelson R. A., Alexander T., Crenshaw D., M., Kaspi S., Malkan M. A., Peterson B. M., Warwick R. S., Clavel, J. et al. 1996, ApJ 470, 364
- Edelson R., Nandra K. 1999, ApJ 514, 682
- Elvis M., Plummer D., Schachter J., Fabbiano G. 1992, APJS 80, 257
- Fabbiano G. 1988, ApJ 325, 544
- Giommi P., Tagliaferri G., Beuermann K., Branduardi-Raymont G., Brissenden R., Graser U., Mason K., Mittaz J. et al 1991, ApJ 378, 77
- Hayashida K., Miyamoto S., Kitamoto S., Negor H., Inoue H. 1988, ApJ 500, 642
- Ishisaki Y., Makishima K., Iyomoto N. 1996, ApJ 48, 237
- Ishida. 1991, PhD Thesis, The University of Tokyo
- Iyomoto N., Makishima K., Fukazawa Y., Tashiro M., Ishisaki Y., Nakai N., Taniguchi Y. 1996, PASJ 48, 231
- Iyomoto N., Makishima K., Tashiro M., Inoue S., Kaneda H., Matsumoto Y., Mizuno T. 1998, APJ 503L, 31
- Iyomoto N. 1999, PhD Thesis, The University of Tokyo
- Iyomoto N., Makishima K. 2000, MNRAS submitted
- Kohmura Y. 1994, PhD Thesis, The University of Tokyo
- Kohmura Y. Inoue Y., Aoki T., Ichida M., Itoh M., Kotani T., Tanaka Y., Ishisaki Y. et al. 1994, PASJ 46, L157
- Krolik J. H., Horne K., Kallman T. R., Malkan M. A., Edelson R.A., Kriss G. A. 1991, ApJ 371, 541
- Lawrence A., Watson M.G., Pounds K.A., Elvis M. 1987, Nature 325, 694L
- Lawson A.J., Turner M.J.L. 1997, MNRAS 288, 920L
- Makishima K. 1988, in Physics of Neutron Stars and Black Holes, ed Y. Tanaka (Universal Academy Press, Tokyo) p175
- Makishima K., Ohashi T., Hayashida K., Inoue H., Koyama K., Takano S., Tanaka Y., Yoshida A. et al. 1989, PASJ 41, 697
- Makishima K., Tashiro M., Ebisawa K., Ezawa H., Fukazawa Y., Gunji S., Hirayama M., Idesawa E., et al. 1996, PASJ 48, 171
- McHardy I., Czerny B. 1987, Nature 325, 696M
- Miller B.W. 1995, ApJ 446, 75L
- Ohashi T., Ebisawa K., Fukazawa Y., Hiyoshi K., Horii M., Ikebe Y., Ikeda H., Inoue H., et al. 1996, PASJ 48, 157
- Pounds K.A., McHardy I.M. 1988 in Physics of neutron stars and black holes, ed Y. Tanaka (Universal Academy Press, Tokyo) p.285
- Reeves J.N., Turner M.J.L., Ohashi T., Kii T. 1997, MRNAS 292, 468
- Ritter H. 1990, A&AS 85, 1179
- Simonetti J.H., Cordes J.M., Heeschen D.S. 1985, ApJ 296, 46
- Tananbaum H., Avni Y., Branduardi G., Elvis M., Fabbiano G., Feigelson E., Giacconi R., Henry J.P., Pye J.P., Soltan A., Zamorani G. 1979, ApJ 234L, 9
- Tanaka Y., Inoue H., Holt S.S. 1994, PASJ 46L, 37
- Wandel A., & Mushotzky R.F. 1986, ApJ 306L, 61

Table 1. Log of ASCA observations of RX J0957.9+6903.

ID	Date		GIS Exposure [†]
	Start [*]	End [*]	
1	93/04/05 06:00	04/06 00:53	32745
2	93/04/07 05:55	04/07 22:11	32065
3	93/04/16 22:40	04/18 17:06	88853
4	93/04/25 14:15	04/25 22:05	12466
5	93/05/01 22:17	05/02 14:11	24145
6	93/05/18 20:48	05/19 20:31	40430
7	93/10/24 14:33	10/25 14:21	43548
8	94/04/01 05:08	04/02 03:21	38087
9	94/10/21 04:25	10/22 07:41	48263
10	95/04/01 18:50	04/02 23:11	21428
11	95/10/24 18:40	10/25 22:51	36443
12	96/04/16 05:34	04/17 09:47	48449
13	96/10/27 04:13	10/28 05:25	32858
14	97/05/08 12:24	05/09 16:20	50197
15	98/04/10 06:18	04/11 10:26	48872
16	98/10/20 19:54	10/21 23:11	23124

* The start and the end time of the observation, in year/month/day hour:minutes and month/day hour:minutes, respectively.

† Exposure time in seconds after the data screening.

Table 2. Model fits to the average 0.7-10 keV spectrum of RX J0957.9+6903*.

	Power-law	Bremsstrahlung
Photon Index or kT (keV)	1.58 (1.55-1.61)	12.0 (11.3-12.8)
N_{H} (10^{21}cm^{-2}) [†]	0.96 (0.72-1.2)	0.41 (fixed)
normalization [‡]	8.64 (8.50-8.78)	2.19 (2.18-2.21)
$\chi^2/\text{d.o.f.}$	66/72	55/73

* The numbers in parenthesis represent the 90% confidence range.

† The Galactic line-of-sight absorption value for the bremsstrahlung model.

‡ Flux (in units of $10^{-12}\text{erg cm}^{-2}\text{s}^{-1}$) over the 2–10 keV energy range for the power-law model, and normalization ($\times 10^{-3}$) of the *bremss* model in *xspec* 10.0.

Table 3. The results of the past observations of RX J0957.9+6903.

Instrument	Date	band [keV]	flux*
Einstein IPC [†]	1979 Apr 27	0.2–4	4.1
Einstein HRI [†]	1979 May 3	0.2–4	3.5
EXOSAT CMA [†]	1983-1986	0.05–2.0	1.0
ROSAT PSPC [‡]	1991 Mar 25	0.5–2.0	2.0 ± 0.1
	1991 Oct 16	0.5–2.0	2.7 ± 0.1
	1992 Sep 29	0.5–2.0	1.7 ± 0.1
ASCA GIS [¶]	1993–1999	0.2–4	6.3 ± 0.1
		0.05–2.0	3.3 ± 0.1
		0.5–2.0	3.1 ± 0.1

* In units of 10^{-12} erg cm⁻² s⁻¹.

† Einstein and EXOSAT results quoted from Fabbiano (1988),
Giommo et al. 1991, respectively.

‡ Assuming the power-law model with the free absorption and photon index.

¶ Assuming the absorbed power-law model with the best fit parameters
in table 2.

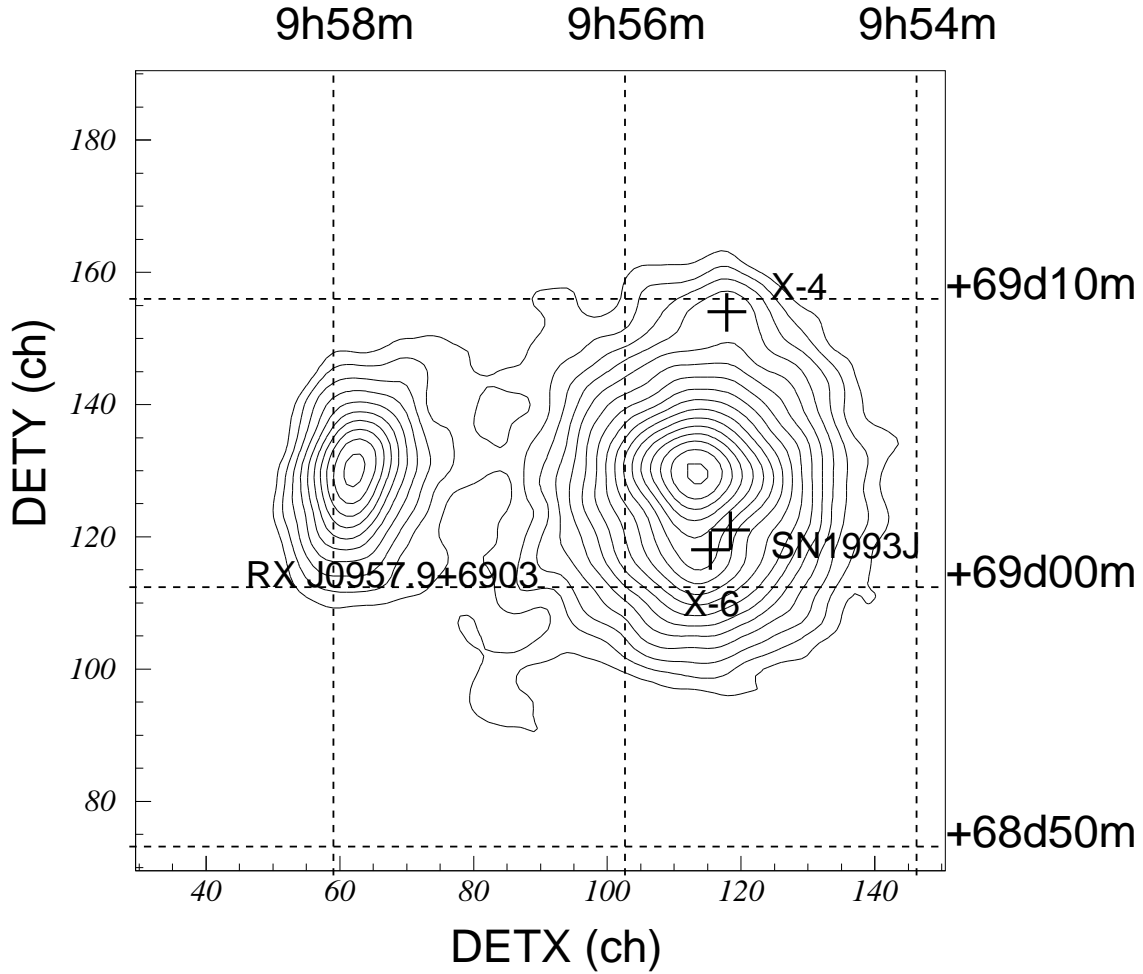


Fig. 1. The 0.7–10 keV X-ray image of the M81 region obtained by summing the GIS2 + GIS3 data for the 7th - 9th observation and smoothing with a Gaussian distribution of $\sigma = 30''$. The background is included, and the image is not corrected for vignetting. The contour level are logarithmic. Sky coordinates are J2000. The crosses represent the X-ray location of SN1993J, X-6 and X-4.

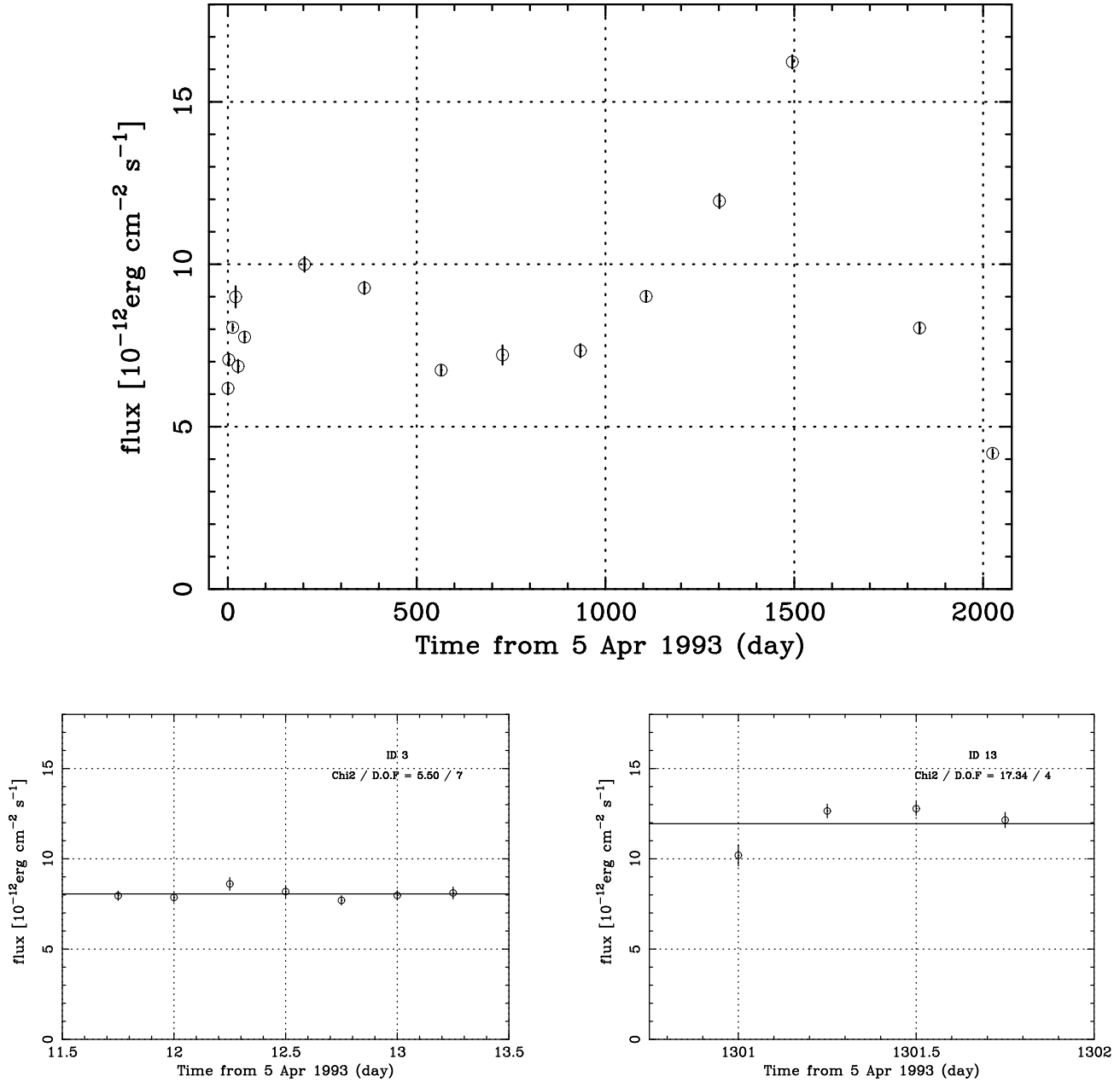


Fig 2. (a) Long-term light curves of RX J0957.9+6903 binned into each observation, 1st - 16th, obtained with GIS2+GIS3. The error bars correspond to the Poisson error. Note that the flux is determined from the spectrum of each observation in terms of an absorbed power-law model. The photon index and absorption column density are free for all the spectra, except the 16th observation in which the absorption was fixed at the Galactic value (see text).

(b) Two examples of short-term light curves of RX J0957.9+6903 with 1/4-day bin, obtained with GIS2+GIS3. The error bars correspond to the Poisson error. The left panel is in the longest 3rd observation. The right panel is in the 13th observation when the short-term variability was maximum, 25%. Also the χ^2 value and d.o.f. calculated against the hypothesis of constant intensity are shown in the top right of each panel. The solid line shows the average of each observation.

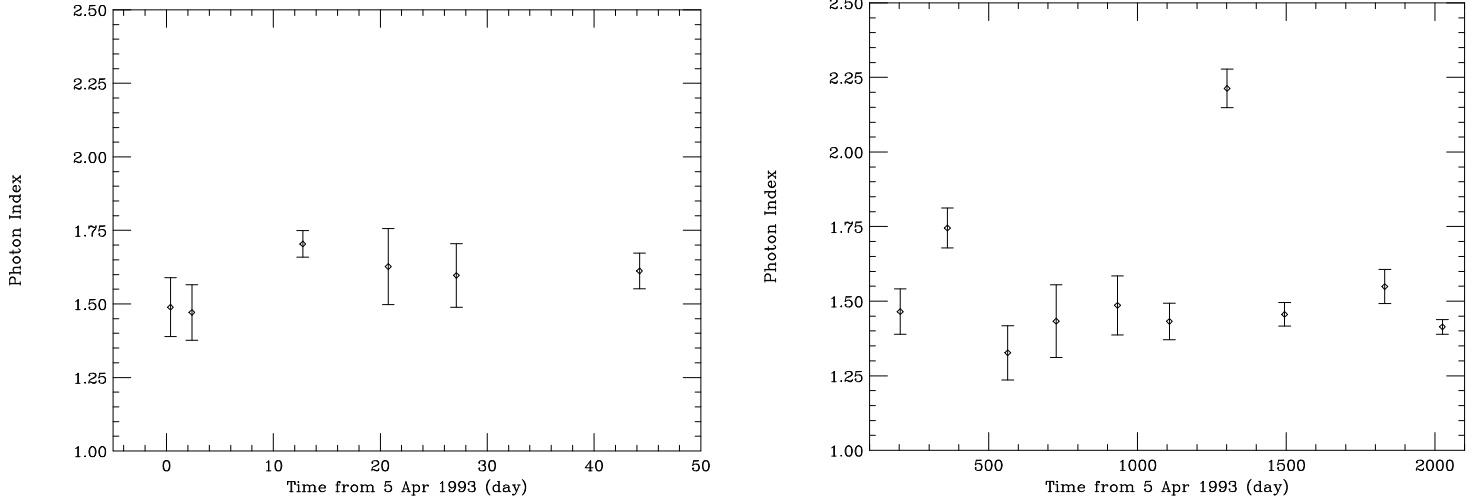


Fig 3. Variability of photon index Γ with 90% confidence errors. The fitting model is an absorbed power-law. Absorption and photon index are taken as free parameters except 16th observation in which the absorption is fixed at the Galactic value. The left and right panels show results from the 1st to 6th and 7th to 16th observations, respectively. Note the difference in time scale.

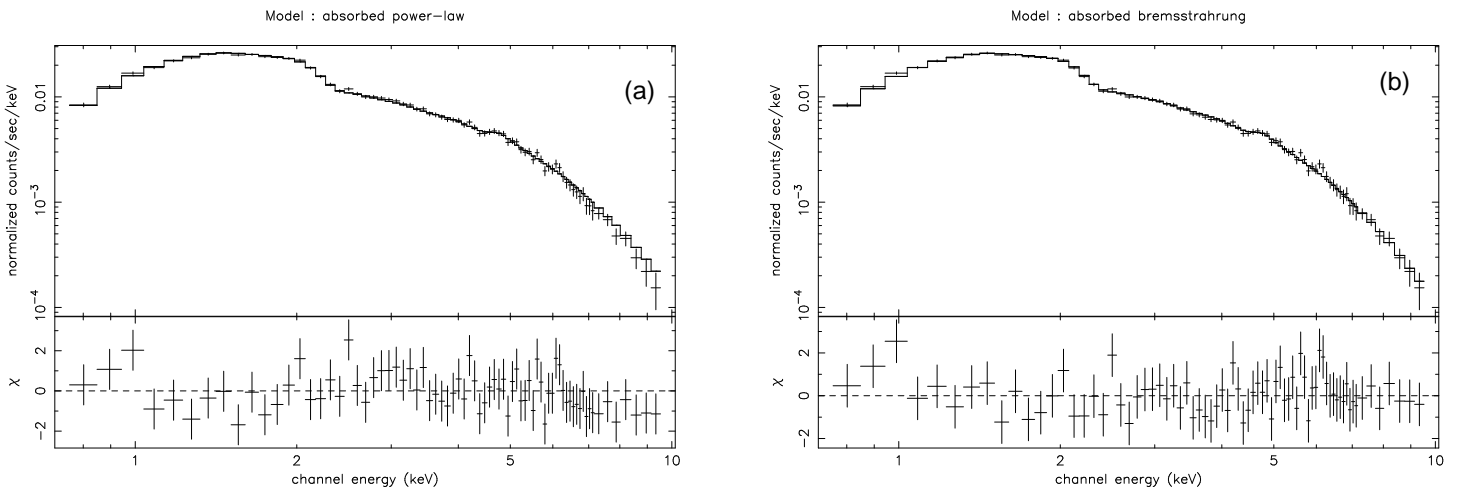


Fig 4. The GIS spectrum of RX J0957.9+6903 in the 0.7-10 keV band, summed over observations 1-16 except 13 and 16. The solid line shows the best-fit power-law model (panel a) and bremsstrahlung model (panel b) convolved through respective instrumental responses. The fit residuals are shown in lower panels.

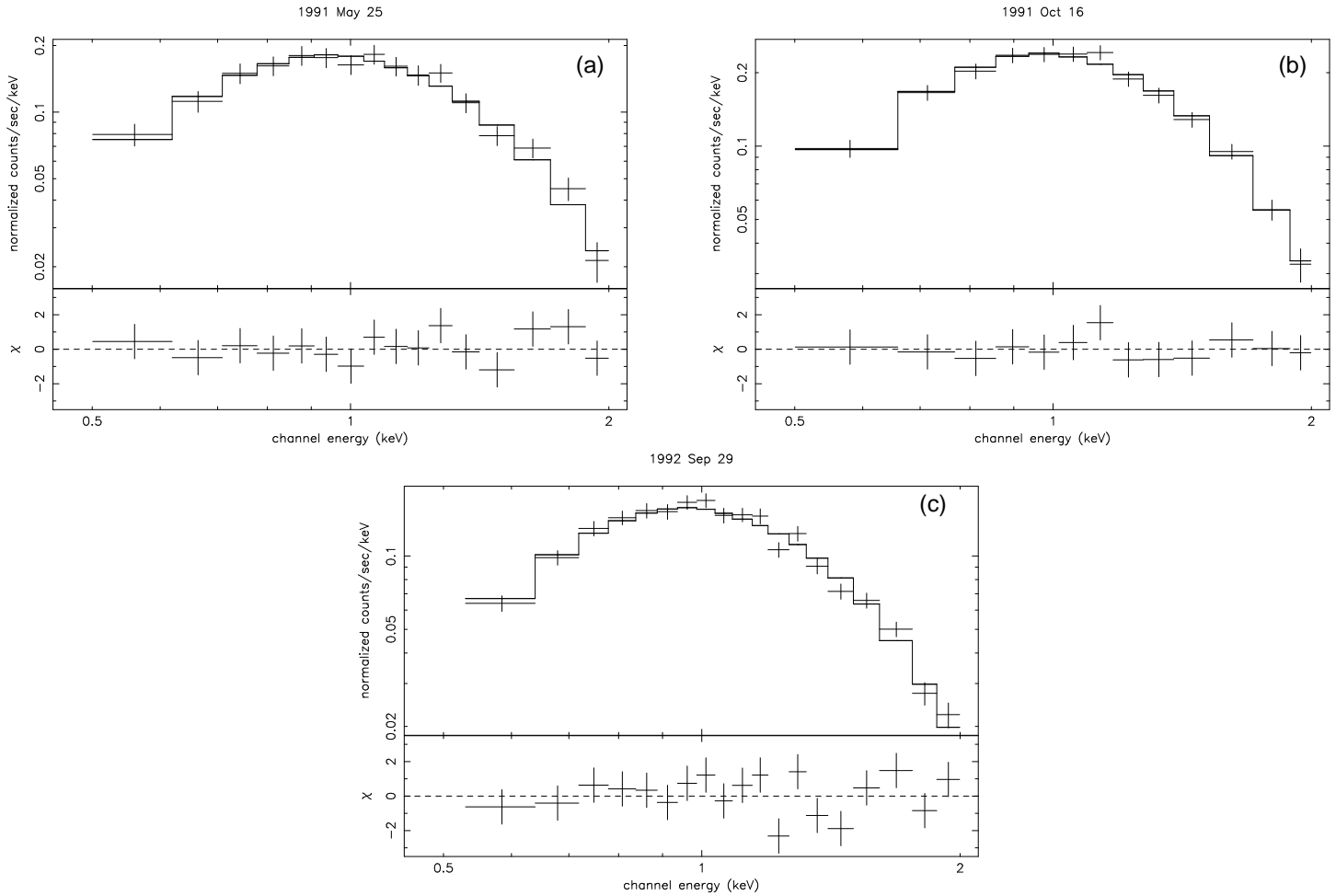


Fig 5. PSPC spectra of RX J0957.9+6903 in the 0.5-2.0 keV band, obtained on 1991 May 25 (panel a), October 16 (panel b) and 1992 September 29 (panel c). The solid line shows the best-fit power-law model convolved through the instrumental response. The fit residuals are shown in lower panels.

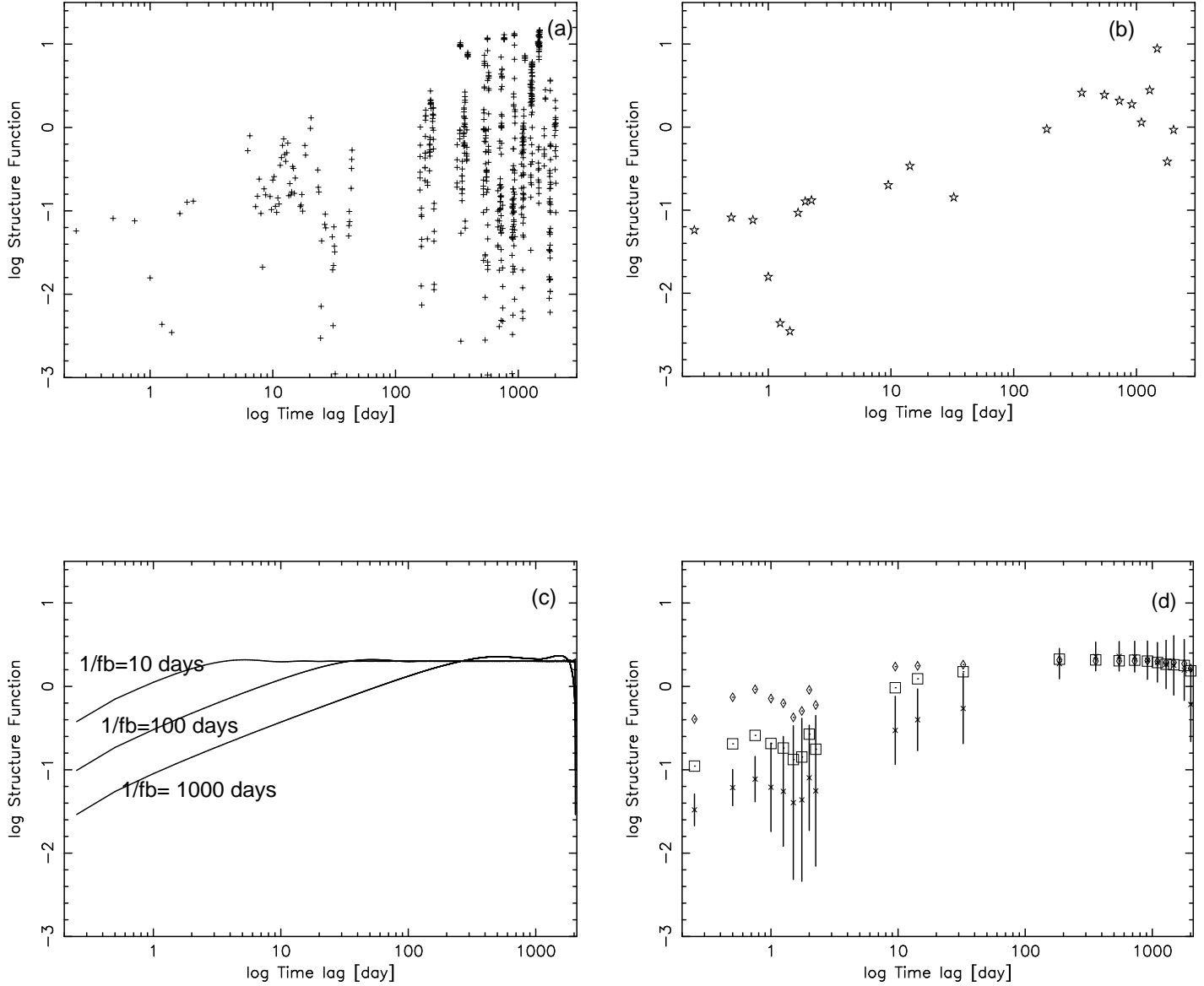


Fig 6. (a) SF of RX J0957.9+6903 before binning. (b) SF after binning. (c) Ensemble average of 1000 fake SFs without window function, generated from the PSD having $\alpha = -1.55$ and $1/f_b = 10, 100$ and 1000 days. (d) Ensemble average of 1000 fake SFs after applying the window function and binning, generated from the same PSD as (c). Diamond, square and cross shows $1/f_b = 10, 100$ and 1000 days, respectively. Only for cross points, we display error bars, which are dispersions among the 1000 simulations.

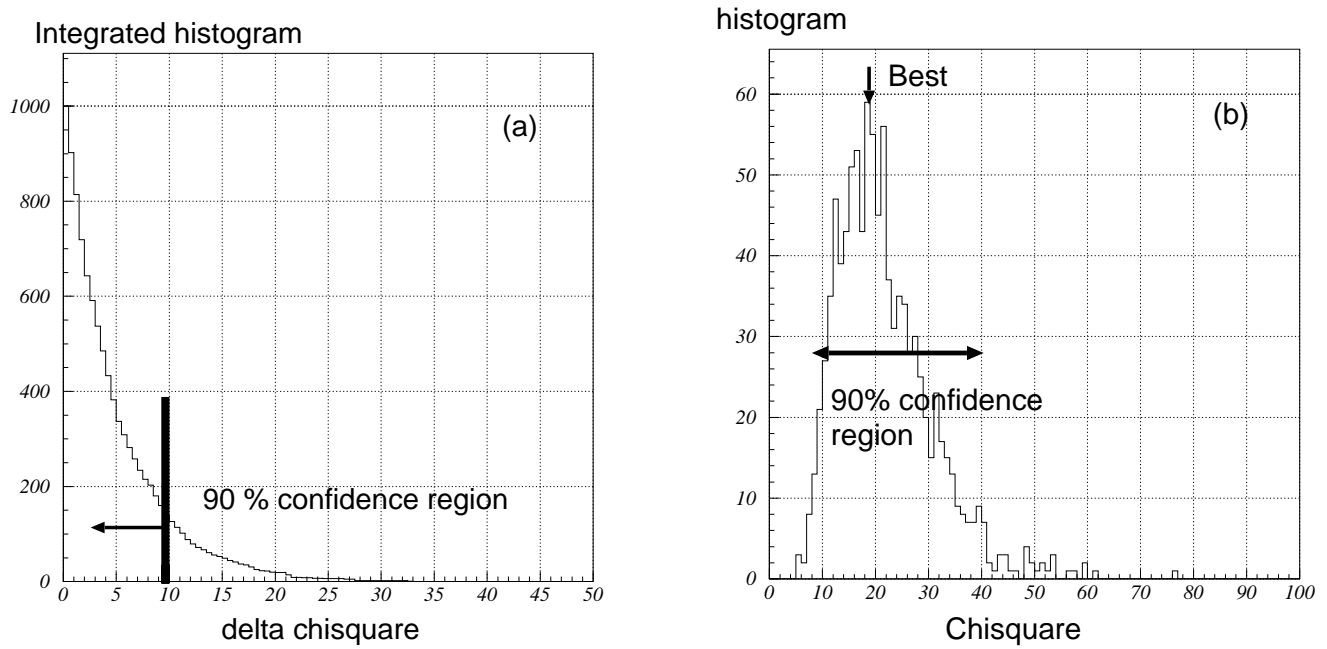


Fig 7. (a) The integrated distribution of $\Delta\chi^2 = \chi^2_{\text{true}} - \chi^2_{\text{min}}$ of 1000 simulated light curves for $1/f_b = 10^{3.2}$ day and $\alpha = -1.55$. (b) The χ^2 distribution of 1000 fake light curves (histogram) and the χ^2 at the best parameters of f_b and α (arrow). Note that degree of freedom of the binned SF is 22.

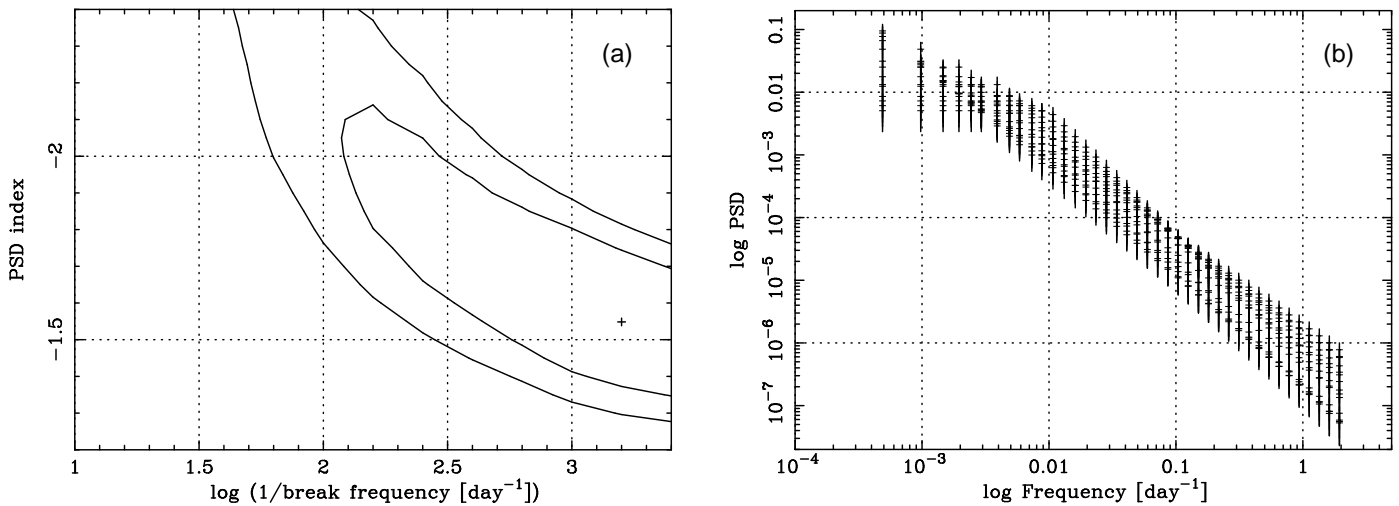


Fig 8. (a) 90% and 99% confidence regions in the 2-dimension plane of f_b and α . The cross represents the best fit parameters from the 1/4-day binned light curve of RX J0957.9+6903. (b) Estimated PSD corresponding to the 90% confidence region of panel (a).